Metamaterial filters at optical-infrared frequencies

Jean-Baptiste Brueckner, Judikaël Le Rouzo, Ludovic Escoubas, Gerard Berginc, Olivier Calvo-Perez, Nicolas Vukadinovic, François Flory

Metamaterial filters at optical-infrared frequencies

Jean-Baptiste Brückner,[1,*] Judikaël Le Rouzo,[1] Ludovic Escoubas,[1] Gérard Berginc,[2] Olivier Calvo-Perez,[3] Nicolas Vukadinovic,[3] and François Flory[1,4]

[1]*Aix-Marseille Université, Institut Matériaux Microélectronique Nanosciences de Provence - IM2NP, CNRS-UMR 6242, Domaine Universitaire de Saint-Jérôme, Service 231, 13397 Marseille Cedex20, France*
[2]*THALES Optronique SA, 2 Avenue Gay Lussac, Elancourt, France*
[3]*Dassault Aviation, 78 quai Marcel Dassault, F-92552 St-Cloud, France*
[4]*Ecole Centrale Marseille, IM2NP CNRS-UMR6242, Technopôle de Château-Gombert, 38 rue Frédéric Joliot Curie, 13451 Marseille Cedex20, France*
[*]*jean-baptiste.bruckner@im2np.fr*

Abstract: We propose two distinctive designs of metamaterials demonstrating filtering functions in the visible and near infrared region. Since the emissivity is related to the absorption of a material, these filters would then offer a high emissivity in the visible and near infrared, and a low one beyond those wavelengths. Usually, such a system find their applications in the thermo-photovoltaics field as it can find as well a particular interest in optoelectronics, especially for optical detection. Numerical analysis has been performed on common metamaterial designs: a perforated metallic plate and a metallic cross grating. Through all these structures, we have demonstrated the various physical phenomena contributing to a reduction in the reflectivity in the optical and near infrared region. By showing realistic geometric parameters, the structures were not only designed to demonstrate an optical filtering function but were also meant to be feasible on large surfaces by lithographic methods such as micro contact printing or nano-imprint lithography.

OCIS codes: (160.3918) Metamaterials; (130.7408) Wavelength filtering devices; (260.2110) Electromagnetic optics.

References and links

1. B. A. Munk, in *Frequency Selective Surfaces* (John Wiley and Sons, 2000).
2. G. R. Fowles, in *Introduction to Modern Optics 2nd ed.* (Dover Publications, 1989).
3. W. H. Emerson, "Electromagnetic wave absorbers and anechoid chambers through the years," IEEE Trans. Antenn. Propag. **21**(4), 484–490 (1973).
4. H. A. MacLeod, in *Thin-Film Optical Filters, 4th ed.* (T. and Francis Ed. 2010), p. 668.
5. J. B. Pendry, A. J. Holden, W. J. Stewart, and I. Youngs, "Extremely low frequency plasmons in metallic mesostructures," Phys. Rev. Lett. **76**(25), 4773–4776 (1996).
6. V. G. Veselago, "The electrodynamics of substances with simultaneously negative values of ε and μ," Sov. Phys. Usp. **10**(4), 509–514 (1968).
7. D. Schurig, J. J. Mock, B. J. Justice, S. A. Cummer, J. B. Pendry, A. F. Starr, and D. R. Smith, "Metamaterial electromagnetic cloak at microwave frequencies," Science **314**(5801), 977–980 (2006).
8. J. B. Pendry, "Negative refraction makes a perfect lens," Phys. Rev. Lett. **85**(18), 3966–3969 (2000).
9. Z. Liu, H. Lee, Y. Xiong, C. Sun, and X. Zhang, "Far-field optical hyperlens magnifying sub-diffraction-limited objects," Science **315**(5819), 1686 (2007).
10. N. I. Landy, S. Sajuyigbe, J. J. Mock, D. R. Smith, and W. J. Padilla, "Perfect metamaterial absorber," Phys. Rev. Lett. **100**(20), 207402 (2008).
11. Y. Avitzour, Y. A. Urzhumov, and G. Shvets, "Wide-angle infrared absorber based on a negative index plsamonic metamaterial," Phys. Rev. B **79**(4), 045131 (2009).
12. G. Berginc, "Structured surfaces and applications," Int. J. Mater. Prod. Tec. **34**(4), 371–383 (2009).
13. W. Cai and V. Shalaev, in *Optical Metamaterials: Fundamentals and Applications* (Springer, 2009).
14. L. Escoubas, R. Bouffaron, V. Brissonneau, J. J. Simon, G. Berginc, F. Flory, and P. Torchio, "Sand-castle biperiodic pattern for spectral and angular broadening of antireflective properties," Opt. Lett. **35**(9), 1455–1457 (2010).
15. H. Butt, R. Rajesekharan, Q. Dai, S. Sarfraz, R. Vasant Kumar, G. A. J. Amaratunga, and T. D. Wilkinson, "Cylindrical Fresnel lenses based on carbon nanotube forests," Appl. Phys. Lett. **101**(24), 243116 (2012).

#186408 - $15.00 USD Received 5 Mar 2013; revised 30 May 2013; accepted 28 Jun 2013; published 10 Jul 2013

16. S. Vedraine, P. Torchio, D. Duche, F. Flory, J. J. Simon, J. Le Rouzo, and L. Escoubas, "Intrinsec absorption of plasmonic structures for organic solar cells," Sol. Energy Mater. Sol. Cells **95**, S57–S64 (2011).
17. D. Duche, E. Drouard, J. J. Simon, L. Escoubas, P. Thorchio, J. Le Rouzo, and S. Vedraine, "Light harvesting in organic solar cells," Sol. Energy Mater. Sol. Cells **95**, S18–S25 (2011).
18. S. Chen, H. Cheng, H. Yang, J. Li, X. Duan, C. Gu, and J. Tian, "Polarization insensitive and omnidirectional broadband near perfect planar metamaterial absorber in the near infrared regime," Appl. Phys. Lett. **99**(25), 253104 (2011).
19. Y. Cui, K. H. Fung, J. Xu, H. Ma, Y. Jin, S. He, and N. X. Fang, "Ultrabroadband light absorption by a sawtooth anisotropic metamaterial slab," Nano Lett. **12**(3), 1443–1447 (2012).
20. X. Liu, T. Tyler, T. Starr, A. F. Starr, N. M. Jokerst, and W. J. Padilla, "Taming the blackbody with infrared metamaterials as selective thermal emitters," Phys. Rev. Lett. **107**(4), 045901 (2011).
21. K. B. Alici, A. B. Turhan, C. M. Soukoulis, and E. Ozbay, "Optically thin composite resonant absorber at the near-infrared band: a polarization independent and spectrally broadband configuration," Opt. Express **19**(15), 14260–14267 (2011).
22. M. Wang, C. Hu, M. Pu, C. Huang, Z. Zhao, Q. Feng, and X. Luo, "Truncated spherical voids for nearly omnidirectional optical absorption," Opt. Express **19**(21), 20642–20649 (2011).
23. P. Bermel, M. Ghebrebrhan, M. Harradon, Y. X. Yeng, I. Celanovic, J. D. Joannopoulos, and M. Soljacic, "Tailoring photonic metamaterial resonances for thermal radiation," Nanoscale Res. Lett. **6**(1), 549 (2011).
24. C. Caloz and T. Itoh, in *Electromagnetic metamaterials: transmission line theory and microwave applications: the engineering approach* (John Wiley and Sons, 2006).
25. L. C. Trintinilia and H. Ling, "Integral equation modeling of multilayered doubly-periodic lossy structures using periodic boundary condition and a connection scheme," IEEE Trans. Antenn. Propag. **52**(9), 2253–2261 (2004).
26. S. Nosal, P. Soudais, and J. J. Greffet, "Integral Equation Modeling of doubly periodic Structures with an Efficient PMCHWT Formulation," IEEE Trans. Antenn. Propag. **60**(1), 292–300 (2012).
27. A. Andryieuski and A. V. Lavrinenko, "Graphene metamaterials based tunable terahertz absorber: effective surface conductivity approach," Opt. Express **21**(7), 9144–9155 (2013).
28. R. Malureanu, M. Zalkovskij, Z. Song, C. Gritti, A. Andryieuski, Q. He, L. Zhou, P. U. Jepsen, and A. V. Lavrinenko, "A new method for obtaining transparent electrodes," Opt. Express **20**(20), 22770–22782 (2012).
29. G. V. Eleftheriades, "EM transmission-line metamaterials," Mater. Today **12**(3), 30–41 (2009).
30. N. I. Landy, C. M. Bingham, T. Tyler, N. Jokerst, D. R. Smith, and W. J. Padilla, "Design, theory and measurement of a polarization-insensitive absorber for terahertz imaging," Phys. Rev. B **79**(12), 125104 (2009).
31. H. Tao, M. Bingham, C. Strikwerda, D. Pilon, D. Shrekenhamer, N. I. Landy, K. Fan, X. Zhang, W. J. Padilla, and R. D. Averitt, "Highly flexible wide angle of incidence terahertz metamaterial absorber: Design, fabrication, and characterization," Phys. Rev. B **78**(24), 241103 (2008).
32. N. Liu, M. Mesch, T. Weiss, M. Hentschel, and H. Giessen, "Infrared perfect absorber and its application as plasmonic sensor," Nano Lett. **10**(7), 2342–2348 (2010).
33. S. Chou, P. Krauss, and P. Renstrom, "Nanoimprint lithography," J. Vac. Sci. Technol. **14**, 4219–4233 (1996).
34. T. Whidden, D. Ferry, M. Kozicki, E. Kim, A. Kumar, J. Wilbur, and G. Whitesides, "Pattern transfer to silicon by microcontact printing and RIE," Nanotechnology **7**(4), 447–451 (1996).
35. P. St John and H. Graighead, "Microcontact printing and pattern transfer using trichlorosilanes on oxide substrates," Appl. Phys. Lett. **68**(7), 1022–1024 (1996).
36. A. Taflove and S. Hagness, in *Computational Electrodynamics: The Finite-Difference Time-Domain Method 2nd ed.* (Artech House, 2000).
37. E. D. Palik, in *Handbook of Optical Constants 1* (Academic Press, 1985), pp. 555–568.
38. T. W. Ebbesen, H. J. Lezec, H. F. Ghaemi, T. Thio, and P. A. Wolff, "Extraordinary optical transmission through sub-wavelength hole arrays," Nature **391**(6668), 667–669 (1998).
39. F. I. Baïda and D. Van Labeke, "Light transmission by sub-wavelength annular aperture arrays in metallic films," Opt. Commun. **209**(1-3), 17–22 (2002).
40. J. R. Sambles, G. W. Bradbery, and F. Z. Yang, "Optical excitation of surface plasmons-an introduction," Contemp. Phys. **32**(3), 173–183 (1991).
41. C. García-Meca, R. Ortuño, R. Salvador, A. Martínez, and J. Martí, "Low-loss single-layer metamaterial with negative index of refraction at visible wavelengths," Opt. Express **15**(15), 9320–9325 (2007).
42. T. Koschny, P. Markos, D. R. Smith, and C. M. Soukoulis, "Resonant and antiresonant frequency dependence of the effective parameters of metamaterials," Phys. Rev. E Stat. Nonlin. Soft Matter Phys. **68**(6), 065602 (2003).
43. G. T. Ruck, D. E. Barrick, W. D. Stuart, and C. K. Krichbaum, in *Radar Cross Section* (Handbook Plenum Press, 1970).
44. X. L. Liu, T. Starr, A. F. Starr, and W. J. Padilla, "Infrared Spatial and Frequency selective metamaterial with near-unity absorbance," Phys. Rev. Lett. **104**(20), 207403 (2010).

1. Introduction

Throughout this paper, optical filtering function is sought. The filter has the ambition to demonstrate a reflectivity less than 15% in the visible region (0.38-0.75 µm), near infrared region (NIR: 0.7-1.5 µm) and short wavelength infrared region (SWIR: 1.5-2.5 µm). A greater than 90% reflectivity has to be achieved simultaneously in the mid wavelength infrared region (3-5 µm) and long wavelength infrared region (LWIR: 8-15 µm). Since the

#186408 - $15.00 USD Received 5 Mar 2013; revised 30 May 2013; accepted 28 Jun 2013; published 10 Jul 2013

antireflective band sought here is large, this optical response is difficult to achieve. Thus we may say that a 15% and a 90% reflectivity are a low and a high reflectivity respectively, suitable for the needs of the targeted applications. Particular interest is found for optical signature reduction, as stealth is an important matter in the optical to SWIR region [1]. It should be noted that the optical response in the 5-8 µm region is not useful for those applications, as the atmospheric transmission is low in this spectral band. Furthermore, the optical filter might be applied onto a metallic ground plane, such as the surface of an airplane, for instance. In this case, transmission is zero. As the sum of absorption, reflection and transmission is equal to 1, the filter will thus be efficient in the visible-near infrared regions by showing either antireflective properties or high absorption mechanisms. Following Kirchhoff's law saying that absorption is almost equivalent to the emitted power at a given temperature [2], such a system would then offer a high emissivity in the visible and near infrared, and a low one beyond those wavelengths. As it acts as a selective thermal emitter, it finds application in the field of thermophotovoltaics, where the goal is to convert radiation from the visible up to 2.5 µm into electrons, while limiting the emissivity for the longer wavelengths. Furthermore, undesired radiation from antennas could be reduced as well with such properties [3]. The optical specifications are then depicted in Fig. 1.

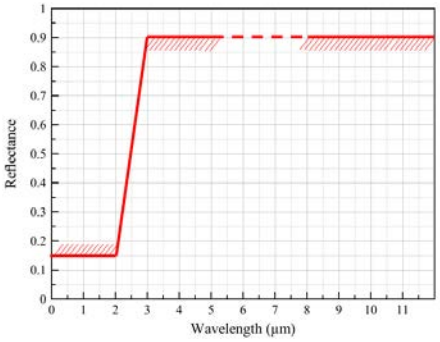

Fig. 1. Optical specifications of the optical filter. Low reflectivity has to be achieved from visible up to 2.5 µm and a mirror-like behavior from 3 to 12 µm.

To achieve complex optical functions, optical thin films have been widely used almost since the beginning of optics [4]. Nonetheless, because of the interferences created by stacking multiple thin layers, an oscillating behavior of the optical response is often obtained, far from the flat one expected on Fig. 1. Furthermore, those stacks may not offer a high thermal and mechanical durability.

However, alternate solutions arise from the emergence of metamaterials. Indeed, those periodically structured-to-the-subwavelength-scale materials generally lead to extraordinary electromagnetic properties unexpected at the natural state [5]. So far, one of the most remarkable features was the demonstration of a negative refractive index, leading to abnormal properties such as negative refraction, evanescent wave's amplification, Doppler and Cerenkov effects inversion [6].

Thus, metamaterials have contributed to the development of new applications such as invisibility cloaking [7], perfect lenses [8], hyperlenses [9], and more recently, electromagnetic wave absorbers, operating from microwave to visible region [10–12].

Principle feature of a metamaterial is that one can control the electric and magnetic response of an electromagnetic radiation by tuning its geometrical parameters [13]. The design has then to be wisely chosen, as it may lead to different optical functions. Low reflectivity can be achieved from a gradient change of the index [14], nanoscale surface roughness [15] or through absorption mechanisms occurring, for instance, in photonic crystals [16] or plasmonic structures [17].

Absorption band for the middle infrared range has been demonstrated with metal stripes [18], or metal/dielectric pyramidal stack [19]. It has also been shown that obtaining multiple

#186408 - $15.00 USD Received 5 Mar 2013; revised 30 May 2013; accepted 28 Jun 2013; published 10 Jul 2013

absorption bands is possible by serializing patterns of different sizes [20]. Furthermore, with two consecutive structures showing slightly different geometrical parameters, a broad absorption band can be achieved. Unfortunately, the drawback of such design, besides it is more time and memory consuming for electromagnetic calculations, the overall efficiency of the absorption band is reduced [21]. Other works on golden split ring resonators showed that it was possible to obtain a nearly 90% high absorption over a 500 nm wide band in the near infrared.

Finally and in the spectral range that interests us, namely the range of the wavelength comprised between 0.5 and 2 µm, perforated metal plates demonstrate an acceptable absorption coefficient resulting in an optical response close to our specifications [22,23].

Numerical analysis has been performed on two commonly used periodic designs [Fig. 2], and is the result of the investigations of two different teams working together on the same project. Thus, for each design proposed here, a specific numerical method has been applied depending on the respective skills of each team. It should be noted that among the existing designs, we chose two different metamaterials providing the best compromise between absorption/antireflection in the visible and high reflectivity in the infrared, and ease of fabrication on flexible substrate.

The first design presented here is a perforated screen, a structure equivalent in transmission line theory to a parallel LC circuit, showing infinite impedance at the resonant frequency (transparent behavior) and null impedance beyond (mirror behavior) [24]. The study was performed by DASSAULT team through a 3D bi-periodic integral method [25,26]. The second structure is a metallic cross grating, corresponding to a series LC circuit, showing this time zero impedance at resonance (transparent behavior) and infinite impedance beyond that frequency (mirror behavior). Further analogy with transmission line theory in metamaterial designing is out of the scope of this paper and can be found in the literature [27–29]. This time, the study was performed by the IM2NP-TOSA team with FDTD method. Finally, through a numerical analysis of these two structures, we will demonstrate various physical phenomena contributing to a reduction in the reflectivity in the optical and near infrared region. In both cases, the geometrical parameters of the designs are also chosen to prove a good compromise in terms of manufacturing difficulties as described in the following section.

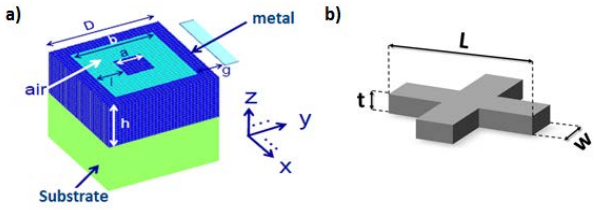

Fig. 2. Unit cells of a coaxial array (a) and a metal cross grating (b).

2. Metamaterial fabrication

Since scaling down the electromagnetic properties to optical or NIR frequencies requires a high resolution fabrication technique, most of the recent works have been achieved by photolithography [30,31], or even with higher resolution technique such as e-beam lithography [32]. Unfortunately, those methods allow fabricating only small area samples restricting greatly the use of the metamaterial for aerospace applications for instance.

2.1 Nanoimprint technology

A design such as the perforated screen can easily be made on a flexible polymer substrate via nanoimprint fabrication technique [33]. This fast, cheap and reproducible elaboration technique is the most suitable as it directly allows fabricating high resolution structures with few processes steps [Fig. 3] and has been the subject of an increasing interest in many fields

#186408 - $15.00 USD Received 5 Mar 2013; revised 30 May 2013; accepted 28 Jun 2013; published 10 Jul 2013

such as biotechnology, chemistry, materials, microfluidics, micro-optics, organic electronics, etc…

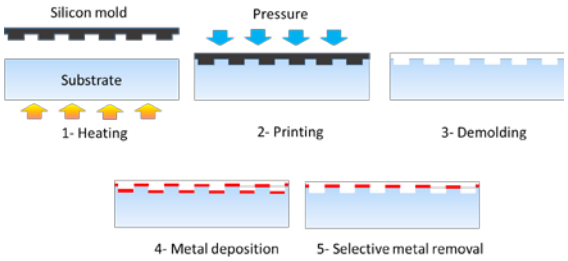

Fig. 3. Schematic view of the steps of nanoimprint fabrication technique.

Once a silicon mold had been fabricated, the patterns are duplicated by printing them onto the heated substrate, which is maintained at a temperature above its melting point in order to render it sufficiently malleable for it to take the shape of the nano-structures present on the mold. The entirety of the substrate is then coated with a metal layer. Depending on the wanted structures, parts of the deposited metal can be selectively removed. Although the resolution achieved with this technology is high, parameters of the patterns have to be greater than 50 nm.

2.2 Microcontact printing technique

As the substrate has to be flat to carry out the metal crosses grating, nanoimprint processes could not be used. Therefore, micro-contact printing (µCP) is a more suitable technique in this case [34,35]. Even though the resolution is not as accurate as the nanoimprint technology, the process is also chosen for its low cost and its capacity to be used on flexible substrate. Principle of this non-optical lithography method is briefly described below and depicted in Fig. 4.

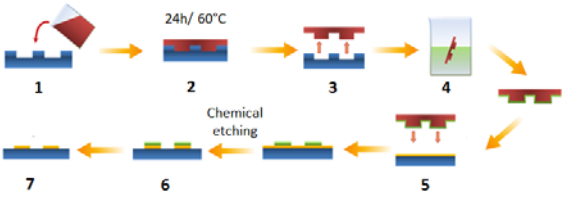

Fig. 4. Principle of micro-contact printing fabrication.

Polydimethylsiloxane (PDMS) polymer is poured on a previously e-beam patterned substrate **(1)**. A 24 hours annealing at 60 °C is generally used to solidify the PDMS buffer **(2)**. After removing it from the silicon substrate **(3)**, the buffer is dipped into octadecanethiol resist solution (ODT **(4)**). The ODT ink is then transferred on the substrate by mechanical contact, forming a pattern according to the buffer one **(5)**. The concentration of the ODT solution will directly be responsible for the length of the spacing between patterns, and generally, a gap smaller than 100 nm is hard to achieve. Thus, further investigated structures will be modeled with the constant gap of 100 nm. After chemical etching, only the patterned metal covered by the ink is remaining **(6)**. The thickness of the structure is directly dependent of the etching duration. However, it is quite hard to achieve structures with thicknesses higher than 100 nm without damaging them. Finally the ODT ink is removed, letting appear only metallic structures on the substrate.

#186408 - $15.00 USD Received 5 Mar 2013; revised 30 May 2013; accepted 28 Jun 2013; published 10 Jul 2013

3. Computational Tools

3.1 Integral method

Electromagnetic calculations on coaxial cable structure [Fig. 2(a)] have been performed with the « 3D-2D periodic » method existing in the SPECTRE code developed by DASSAULT AVIATION aerospace company. This method consists in solving Maxwell's equations in harmonic regime. The outer space of the grating is treated by bi-periodic integral equations and 3D integral equations with pseudo-periodic boundary conditions are used on the inner side, giving access to transmission and reflectivity spectrum of the grating [25,26].

Figure 5 shows an example of a fictional box and a structure included inside. Numerical calculations require a spatial discretization for both box and structure. Mesh is represented as well for those two objects.

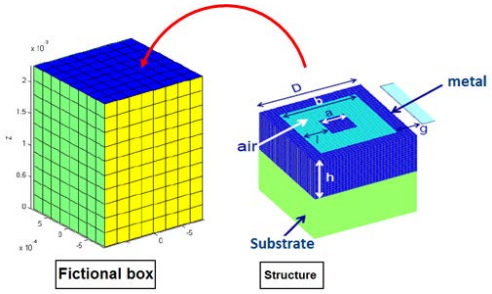

Fig. 5. Fictional box and the included structure, geometry and mesh used in the 3D-2D periodic method from the SPECTRE code.

3.2 Finite Difference Time Domain Method

In order to determine the scattering parameters of the metallic cross grating [Fig. 2(b)], commercial software Lumerical FDTD Solutions is used. Based on spatial and temporal discretization of Maxwell's equations, the Finite Difference Time Domain (FDTD) method is commonly used to solve the propagation of electromagnetic waves in complex structures [36]. The computation requires a geometry definition of the structure, its optical indices of materials n (λ) and k (λ) taken from the work of Palik [37]. Wavelength of the illuminating source and its angle of incidence, calculation domain and a mesh size are also defined [Fig. 6]. The adjustment of the mesh is very important as if it is too thin, the computation time becomes too long. Moreover, if it is too coarse, the risk of not taking into account all physical phenomena is not zero, which can greatly distort the results. Thus, after various convergence tests, non-uniform mesh is used. Periodic conditions are used to repeat periodically the defined pattern along the x and y axis, allowing the simulations of the interactions with neighboring structures.

Finally, a "Perfectly Matched Layer" is set on the top and bottom of the computational domain, simulating a highly absorbent material. Thus, only a negligible energy would be reflected back in this domain.

#186408 - $15.00 USD Received 5 Mar 2013; revised 30 May 2013; accepted 28 Jun 2013; published 10 Jul 2013

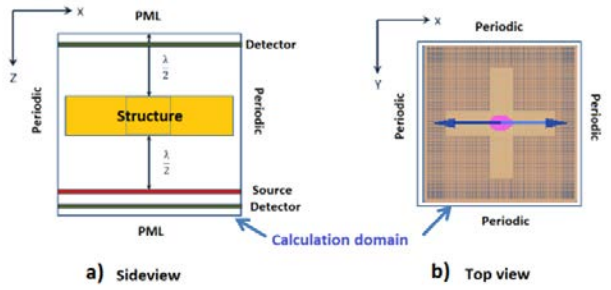

Fig. 6. Sideview of the FDTD calculation domain showing the structure in the center and the front and back detectors giving a measurement of the reflected and transmitted power emitted by the source place at λ/2 of the structure. Perfectly match layers are placed along z on both ends of the domain (a). Mesh is represented in the top-view of the calculation domain (b). Periodic conditions are used along the y and x directions.

To avoid any confusion, only reflectivity spectra will be computed by both numerical methods. Absorption spectra will only be detailed when necessary. Furthermore, this study, performed at normal incidence, constitutes a first step. Obviously, for stealth applications, the angular response is of the utmost importance, and we assume that the optical response might be degraded with a non-zero incidence angle. However we decided in the first place to focus on the optical response of the filters at normal incidence. Even in this simple case, the problem is already difficult to solve since a broad spectral domain is considered. Other designs or solutions taking into account the angular response might be proposed in a future study.

4. Numerical Analysis

4.1 Squared coaxial cables

4.1.1 Context

During the past ten years, the study of the optical properties of metallic perforated screens with hole diameters smaller than the wavelength has experienced high activity, due to non-intuitive experimental results obtained by Ebbessen [38]. Indeed, while the dimensions of the holes prohibit any spread of light, relatively high transmission levels were measured. Many theoretical and experimental works have followed and highlighted the role of plasmons in phenomena called extraordinary transmission. Other structures have been explored to improve the system performance. Van Labeke's team has studied coaxial holes arrays that allow achieving around 90% transmission, through waveguiding inside the cavities [39]. The study presented in this section is based on these results.

4.1.2 Structure description

The structure is described in Fig. 2(a). Dimensions have been optimized to get minimal reflectivity in the visible range, taking into account realistic sizes for nanoimprint technology. A comparison of the spectral dependencies of the electric permittivity and the skin depth of silver and gold shows that gold is more absorbent than silver in the visible (<0.7 µm). Then, only silver based structures are considered (optical indices are taken from Palik [37]). Substrate index is either equal to 1 or 1.5. Dimensions are: D = 280 nm, a = l = g = 70 nm.

In the visible, an oscillation mode of the metal creates the appearance of a wave propagating along the surface. Assuming a planar dielectric/metal interface, plasmon dispersion relation is given as it follows [40]:

$$k_{sp} = \frac{2\pi}{\lambda} n_{diel} \sqrt{\frac{\varepsilon_{metal}}{\varepsilon_{metal} + 1}} \qquad (1)$$

#186408 - $15.00 USD Received 5 Mar 2013; revised 30 May 2013; accepted 28 Jun 2013; published 10 Jul 2013

With k_{sp} the frequency-dependent surface plasmon wave-vector, n_{diel} the optical index of the dielectric and ε_{metal} the permittivity of the metal. For the wave propagation, it requires then $\varepsilon_{metal}<1$. At that moment, $k_{sp}>n_{diel}\omega/c$ and the wave is guided by the interface. One of many ways to excite a plasmon by a plane wave consists in etching very small height periodic patterns on a planar dielectric/metal interface. Diffraction orders of the grating different from zero are then likely to excite the plasmon, following Eq. (2):

$$k_{sp} = k_i + m\frac{2\pi}{D} \tag{2}$$

With m the diffraction order. The grating period D necessary to excite a plasmon at a given wavelength, has been calculated from Eq. (2). For a 0.28 µm period (case studied in this section), the plasmon appears at $\lambda = 0.36$ µm for a vacuum/Ag interface and at $\lambda = 0.46$ µm for a glass/silver interface.

4.1.3 Numerical results

The reflectance, transmission and absorption spectra of the periodic structure coaxial holes are shown in Fig. 7. The lower medium corresponds to vacuum, thus the structure is symmetric: coupling between excited waves in the cavities and the plane waves of the upper and lower media are identical. It was found that for $\lambda = 0.6$ µm, the reflection is almost zero regardless of the metal layer thickness and transmission is high (> 80%) for a 150 nm thick layer. The difference between these two variables corresponds to the absorption by the walls of the coaxial guide, which increases with the thickness of the metal layer. It can be concluded that the impedance of the guided mode in the cavity at $\lambda = 0.6$ µm is close to the impedance of the vacuum/grating interface. For $\lambda<0.4$ µm, the skin depth of silver is greater than 35 nm. However, the width between two slits is equal to 70 nm and the width of the central pillar is equal to 70 nm. Then, the wave penetrates into the metal parts of the periodic structure with a partial lateral attenuation. Therefore it is rapidly absorbed (absorption is independent of the thickness of metal along z).

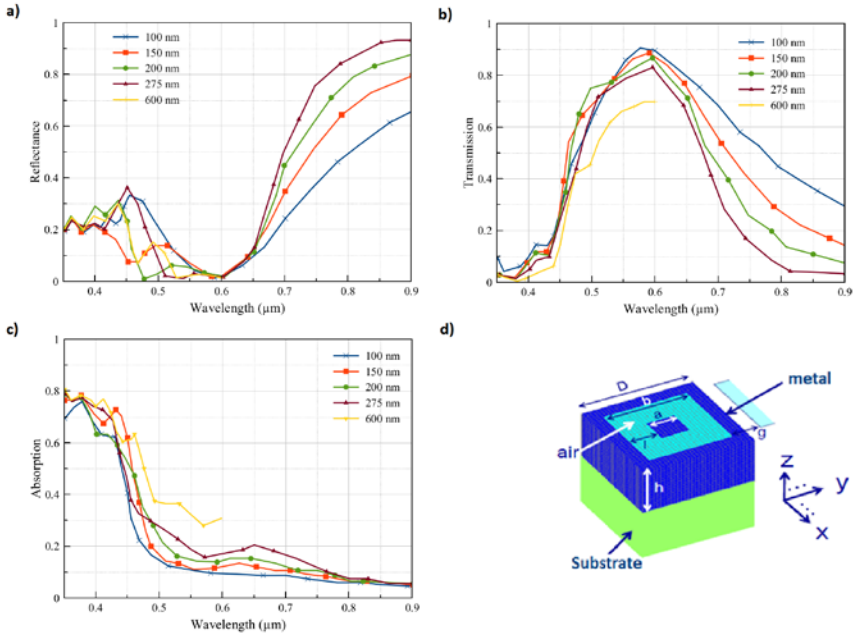

Fig. 7. Reflectance (a), transmission (b) and absorption (c) spectra of the coaxial cable grating (d). The thickness value of the metal layer is varied from 100 to 600 nm. Upper and lower media is vacuum.

#186408 - $15.00 USD Received 5 Mar 2013; revised 30 May 2013; accepted 28 Jun 2013; published 10 Jul 2013

The visualization of the normal field at λ = 0.6 μm on the walls of the cavity allows to appreciate the shape of the guided mode [Fig. 8]. It is similar to a TE11 mode, of guided wavelength of the order of λ = 0.85 μm, very slightly disturbed by the lower interface. The cutoff wavelength of the mode is of the order of λ = 0.84 μm ($1/\lambda_c^2 = 1/\lambda^2 - 1/\lambda_g^2$).

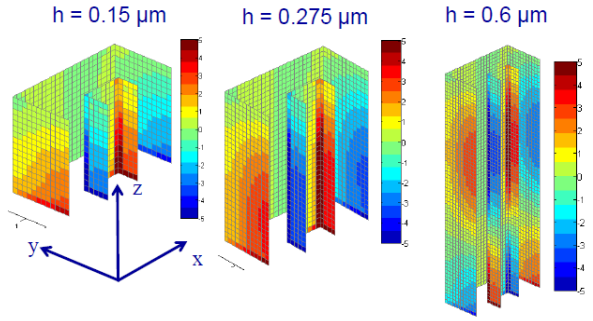

Fig. 8. Real part of the normal Electric field on the walls of the cavity, for different heights at normal incidence and λ = 0.6 μm. Lower medium is vacuum. Incident Electric field propagates along x.

The influence of the lower interface appears on the curves of Fig. 9, including the transmission spectra and absorption. Thus we notice an absorption maximum at λ = 0.5 μm when glass substrate is used, which translates a transmission hole, and which is caused by the appearance of a plasmon on the lower interface, highlighted by a strengthening of the normal field. We also note that, for λ = 0.6 μm, the reflection coefficient is equal to 8%, due to the reflection at the vacuum/glass interface.

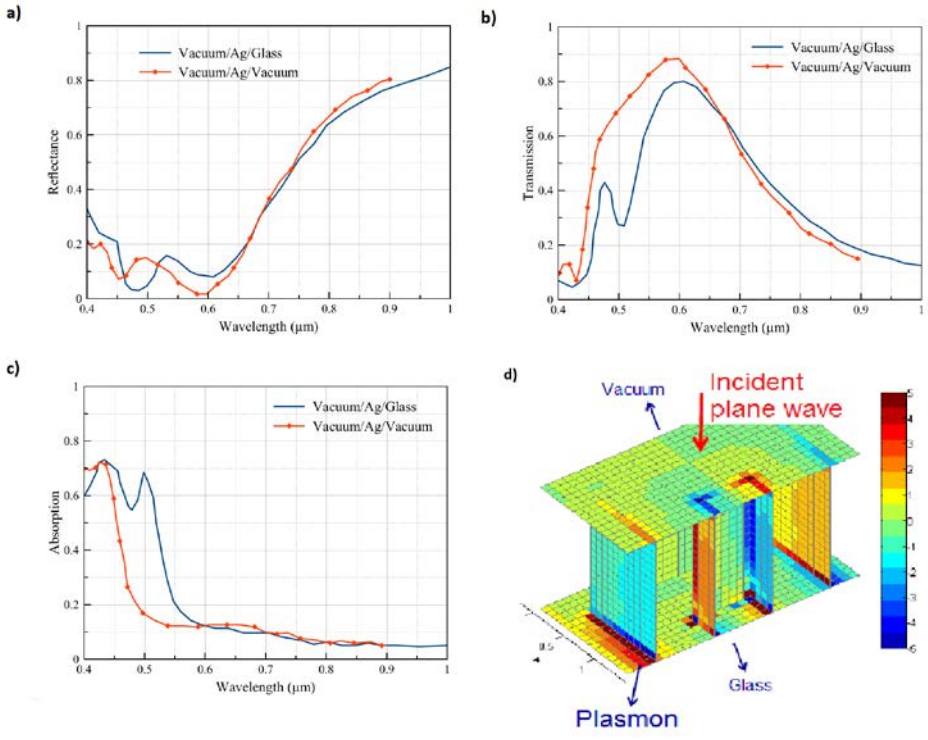

Fig. 9. Effect of the lower medium on reflectance (a), transmission (b) and absorption (c) properties of the structure, and mapping of the normal field intensity at λ = 0.5 μm (d). Thickness of the metal layer is equal to 150 nm.

#186408 - $15.00 USD Received 5 Mar 2013; revised 30 May 2013; accepted 28 Jun 2013; published 10 Jul 2013

To conclude this section, Fig. 10 shows the reflection coefficient of the 150 nm thick periodic structure between 0.4 and 10 µm (index of the substrate n = 1.5). For wavelengths above 2 µm, the reflectance is higher than 96% (2% less than the reflection of a silver non-perforated plate).

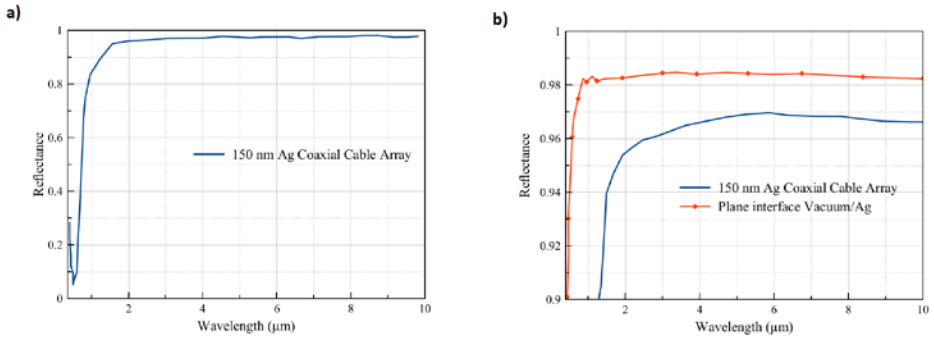

Fig. 10. Reflectance of the 150 nm thick periodic structure with a n = 1.5 substrate (a), and comparison with a non-perforated silver plate (b).

A thick perforated metal screen acts as a thin high-pass filter, which thus meets partially the specifications fixed (infrared reflective structure). However, the reflectivity in the visible-near infrared region is far from the 15% expected. Thus, in order to match the optical specifications, low reflectivity band has to be extended up to 2.5 µm.

4.2 Metal cross grating

Works on theoretical negative index metal stripe, cross and squared crown gratings have demonstrated interesting low band pass filter properties in the visible region [41]. For this study, a silver cross grating has been chosen as its symmetric pattern is insensitive to polarization. Geometrical parameters of the reference structure and reflection and transmission spectra are given in Fig. 11.

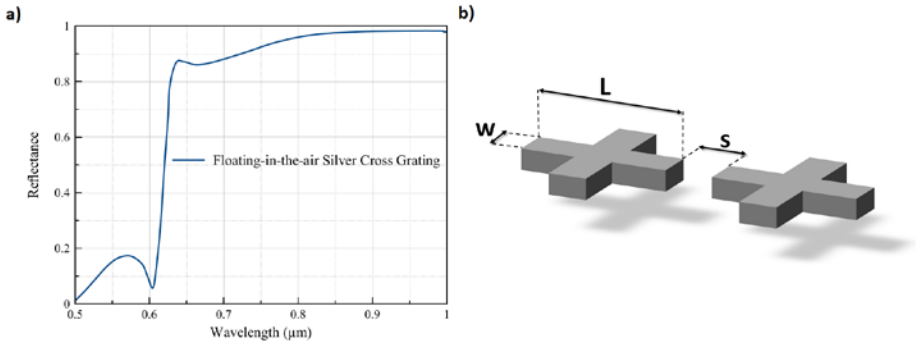

Fig. 11. Reflectance spectrum at normal incidence and in the visible and near infrared region of a silver cross grating floating in vacuum [26] (a) and its parameters: thickness t = 150 nm, width and length of the stripes forming the cross w = 54 nm and L = 266 nm, respectively, and s = 30 nm length of the gap between the structures (b).

In terms of transmission line theory, metallic cross grating corresponds to a LC series circuit, showing zero impedance at resonance (transparent behavior) and infinite impedance beyond that frequency (mirror behavior). Therefore for the reference structure, below 600 nm the structure is almost transparent to incident radiation (a small portion of the light is still reflected at the surface of the crosses). At 640 nm, the electric component of the light strongly

#186408 - $15.00 USD Received 5 Mar 2013; revised 30 May 2013; accepted 28 Jun 2013; published 10 Jul 2013

couples along the crosses, leading to a large drop of transmission. This resonant frequency is strongly dependent on the gap size [42].

Thus, a scaled up floating-in-the-air silver cross grating will be first investigated through FDTD calculations. Afterwards, and in order to better match optical specifications, a metal cross/dielectric spacer/metallic substrate stack will be presented. But first, the most suitable fabrication technique and the resulting constraints have to be discussed beforehand. Those constraints will fix some geometrical parameters of the modeled structures.

4.2.1 Floating-in-the-air silver crosses

Floating-in-the-air silver cross grating is then considered. As the plasma frequency is dependent on the lattice period, moving the reflectivity threshold from the optical region up to 2.5 µm is possible by direct scaling up of the geometric parameters of the crosses. Several structures have then been computed with different sizes [Fig. 12], with L and w parameters varied proportionally while trying to keep geometrical parameters in the range of fabrication technology limits: the gap s and thickness t of the crosses are kept at 100 nm.

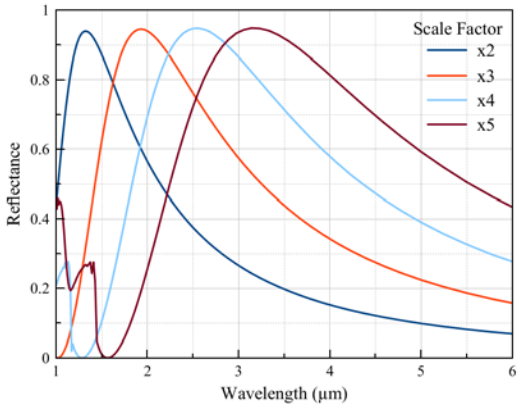

Fig. 12. Reflectance spectra for different scales of floating-in-the-air silver crosses grating from 0.5 to 5 µm range at normal incidence.

A clear shift of the optical response along with the scale of the crosses is noticeable. Reflectance is zero at the resonant wavelength. Below this wavelength, the reflectivity of the grating increase as the crosses scale gets larger. Above the resonance, reflectance strongly increases up to more than 0.9, then collapse as we go further into the infrared. This drop of reflectance is mainly due to insufficient metal fill factor of the unit cell. Therefore, the silver cross grating cannot meet by itself the optical specifications defined in Fig. 1, as reflectance is too high in the near infrared and too low in the mid infrared. However, a solution can be found by coupling a ground plane to the metallic cross grating. This system is then described in the next section.

4.2.2 Metal Cross/Dielectric/Metal stack

It is well known that it is possible to create a resonant wave absorber by placing two metallic sheets at a certain distance [43]. From this principle, work on a three layers metamaterial, pairing golden cross grating to a 100 nm thick gold plate, separated by a dielectric layer has proven a rather large and strong absorption band around 6 µm [44]. This is mainly due to a coupling of the magnetic component of light with both center of the cross and ground plane, generating antiparallel currents that lead to a resonant response of the metamaterial and thus to a near zero reflectivity. This system is interesting in the sense that this magnetic response can be adjusted to our specifications by tuning the geometric parameters of the crosses and their distances from the ground plane. Furthermore, the collapse of the reflectance in the infrared occurring in the previous section is no longer a worry, as long as the metallic back

#186408 - $15.00 USD Received 5 Mar 2013; revised 30 May 2013; accepted 28 Jun 2013; published 10 Jul 2013

plate is thick enough. Nonetheless, using a gold metal plate like in the mentioned works43 can be nocuous for the optical response in the visible and NIR, as the reflectivity would be enhanced in those regions. Thus, we have chosen to use tungsten substrate as this metal is more absorbent than gold in the visible and near infrared [Fig. 13].

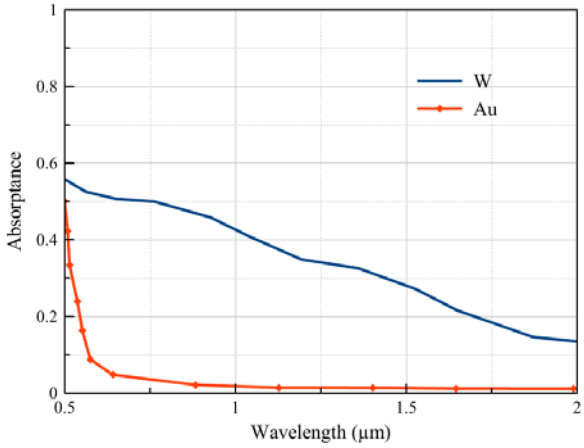

Fig. 13. Absorptance spectra of thick tungsten and gold layers, from 0.5 to 2 μm range and at normal incidence.

A 100 nm thick layer of tungsten is enough to achieve zero transmission for a wavelength range from 0.5 to 10 μm, thus the energy that is not reflected is entirely absorbed by the stack. However, semi-infinite tungsten substrate is used, simplifying the calculations.

To resume the situation, the modeled structure is a silver cross grating resting on a dielectric spacer, laid in its turn on a semi-infinite tungsten substrate [Fig. 14]. Period of the grating and thickness of the dielectric layer are then matched to achieve a near unity absorption around 2.8 μm. The parameters of the silver crosses become: L = 900 nm, w = 150 nm, t = 100 nm and s = 100 nm. The dielectric spacer has constant optical indices n = 1.38, k = 0 and d = 100 nm.

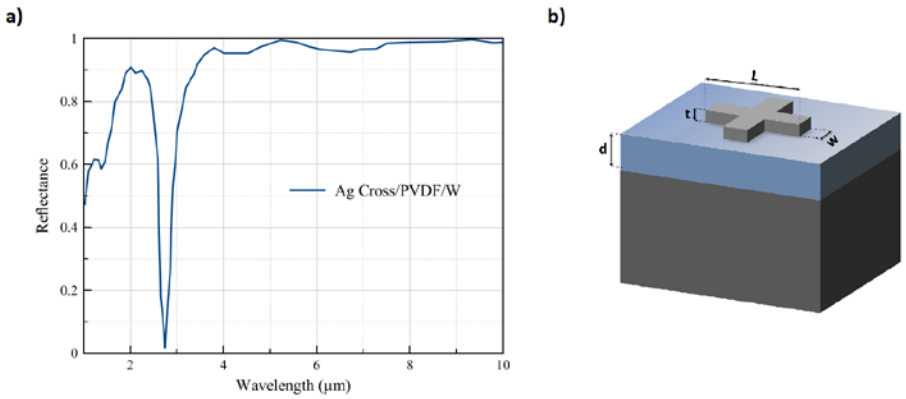

Fig. 14. Reflectance spectrum from 1 to 10 μm range at normal incidence of the three layers stack and unit cell of the modeled grating (a) and its geometric parameters (b).

Despite its strong efficiency, the absorption band is too narrow and consequently, NIR region remains problematic, reflectivity is too high. However by using a lossy dielectric spacer, reflectivity can be reduced in the visible and NIR region. This solution is detailed in the next section.

#186408 - $15.00 USD Received 5 Mar 2013; revised 30 May 2013; accepted 28 Jun 2013; published 10 Jul 2013

4.2.3 Metal Cross/Lossy dielectric/Metal stack

As the extinction coefficient k of a polymer such as, for instance, a commercial Polyvinylidene fluoride (PVDF) is non-zero in the visible and NIR region, losses are attended in the dielectric layer. Geometrical parameters of the silver crosses have to be redefined to offer a good compromise for the optical specifications and become: L = 525 nm, w = 150 nm, t = 50 nm and s = 100 nm. The thickness of the PVDF layer is d = 100 nm, its optical indices used for the calculations as the reflectivity spectrum of the system from 0.5 to 10 µm, are depicted by Fig. 15 a. As the PVDF is supposed to have a zero extinction coefficient in the 3-5 µm and 8-10 µm, computations have been done as well with a dielectric of constant optical indices n = 1.38 and k = 0 [Fig. 16].

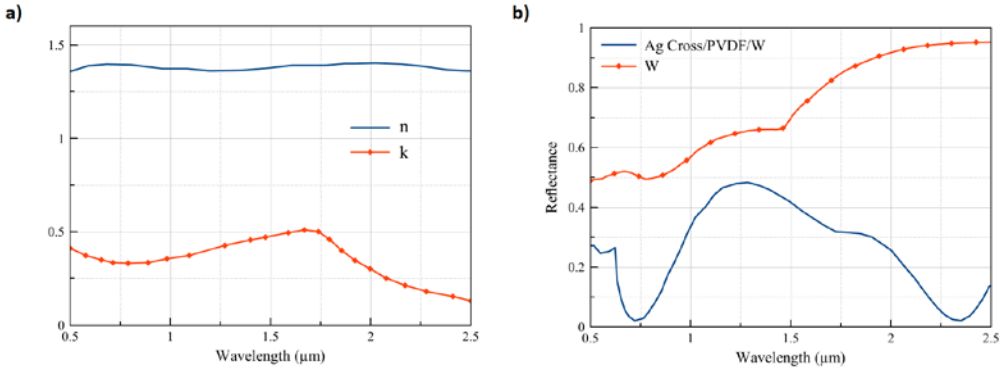

Fig. 15. Optical indices of a commercial Polyvinylidene fluoride from 0.5 to 2.5 µm (a) and reflectance spectrum of the Ag Cross/PVDF/W stack and a semi-infinite thick tungsten layer at normal incidence from 0.5 to 2.5 µm range (b).

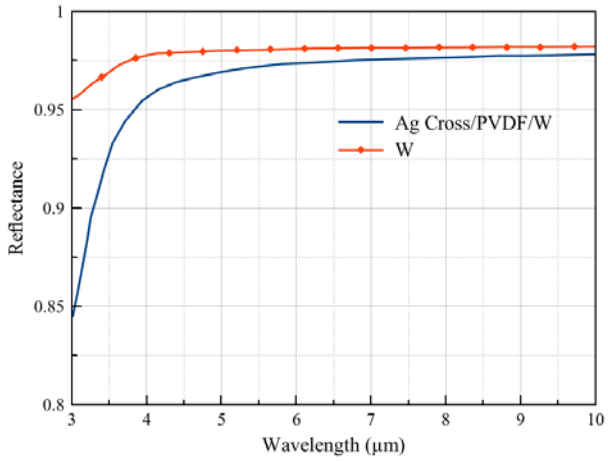

Fig. 16. Reflectivity spectrum of the Ag cross/PVDF/W stack and a semi-infinite thick tungsten layer at normal incidence for the 3-10 µm range.

The visible region's reflectivity has significantly decreased. Two minima of reflectance are obtained around λ = 0.7 µm and λ = 2.3 µm. However, the reflection coefficient is quite high between those two wavelengths, being almost around 0.5 at 1.3 µm. We assume that it is possible to decrease it by using a more absorbent dielectric spacer (Black PVDF for instance). The main drawback in the use of such polymers is that they generally demonstrate a high extinction coefficient all over the spectrum. Thus, despite the improved response in the visible and near infrared, the mirror behavior in the mid infrared region might be damaged.

#186408 - $15.00 USD Received 5 Mar 2013; revised 30 May 2013; accepted 28 Jun 2013; published 10 Jul 2013

Yet another possibility would be to use tungsten crosses instead of silver ones, as this metal shows a good absorption coefficient from $\lambda = 0.5$ to 2 µm. This time, the major difficulty lies within the fabrication technique. Indeed, the chemical etching process would then have to be redefined specifically for this case.

In conclusion, the overall optical response demonstrated in this section has been improved from 0.5 to 2.5 µm range in comparison with a semi-infinite thick tungsten layer [Fig. 15(b)]. The average reflectivity is around 30%, becoming closer to the objectives, but still above the 15% expected, and improvements have to be made in this spectral band in order to meet the specifications. However, compared to the coaxial cable array described in section 3.1 where low reflectivity occurred only in a small portion of the spectrum, the cross/PVDF/Tungsten system has reduced to a significant extent the reflectance over a large band. Concerning the middle infrared regions, as for the coaxial cable array, over 90% reflectance has been achieved for 3-5 µm range, being even over than 96% for the 8-10 µm region.

5. Conclusion

Optical filter function was sought for applications in stealth or thermophotovoltaics domain. Specifications to meet by the proposed systems were to demonstrate low reflectivity from the visible up to 2.5 µm and a mirror behavior above. Moreover, the proposed designed had to be meant for large surface fabrication techniques, such as nanoimprint or microcontact printing, thus realistic parameters had to be taken into account. For this, two types of metamaterial have been designed.

Firstly, a perforated metal plate displaying coaxial cavities has been computed with periodic 3D-2D integral method. It theoretically behaves such as a parallel LC resonant circuit, transparent at the resonance wavelength, or as waveguide. Silver was retained rather than gold because it has fewer losses in the visible. Parameters of the studied structure are such that the maximum transparency is obtained at $\lambda = 0.6$ µm (minimum reflection, less than 0.1). At this wavelength, the propagative TE11 mode excited in each cavity is perfectly adapted to interface with the vacuum. The reflection coefficient R is less than 0.15 between 0.45 and 0.65 µm. The lattice spacing (0.28 µm) leads to the appearance of a surface plasmon at $\lambda = 0.5$ µm, which causes an increase of the absorption and therefore a drop in reflectance and transmission. High reflection coefficient has been achieved in the infrared (> 96%) with only a 150 nm thick silver perforated plate. Despite the optical filtering properties demonstrated by such array, improvements are yet to be done in the NIR and SWIR region as the 15% reflectivity limit fixed by the specifications has been overcome in this spectral band. Therefore, another metamaterial design has been investigated.

Thereafter, a silver cross grating, corresponding to a series LC circuit, showing this time zero impedance at resonance (transparent behavior) and infinite impedance beyond that frequency (mirror behavior) has been investigated through FDTD calculations. Direct scaling has been made to match the frequency range of the optical specifications. Unfortunately high reflectivity could not be maintained in the mid infrared irrespective of the metal thickness used. Using a tungsten ground plane at the back has improved the optical response, and by matching the distance between the cross grating and the ground plane, near unity absorption band has been demonstrated. However, this absorption band was too narrow to meet the specifications and reflectivity kept being too high in the visible and NIR region. With the help of a commercial lossy polymer such as Polyvinylidene fluoride (PVDF), general optical response has been significantly improved, reducing the average reflectivity down to 30% from 0.5 to 2.5 µm, while the tungsten substrate maintained the metamaterial mirror-like behavior in the mid infrared. Even though large band optical filter has been demonstrated, its efficiency in the visible and NIR regions has to be improved, as the reflectivity in this domain becomes at times greater than the 15% specified. For this, the use of a more absorbing polymer could provide better results, or if fabrication process allows it, better optical responses are also to be expected by using tungsten crosses instead of silver ones.

#186408 - $15.00 USD Received 5 Mar 2013; revised 30 May 2013; accepted 28 Jun 2013; published 10 Jul 2013

Acknowledgments

The authors acknowledge the “Agence Nationale de la Recherche” (ANR) for funding the NPOEM project, Cécile Gourgon and the “Laboratoire des Technologies de la Microélectronique” (LTM, UMR 5129, Grenoble) for defining the fabrication constraints.

#186408 - $15.00 USD Received 5 Mar 2013; revised 30 May 2013; accepted 28 Jun 2013; published 10 Jul 2013